ACS APPLIED MATERIALS & INTERFACES

Research Article

www.acsami.org

High-Efficiency BODIPY-Based Organic Photovoltaics

John J. Chen,[†] Sarah M. Conron,[†] Patrick Erwin,[†] Michael Dimitriou,[‡] Kyle McAlahney,[†] and Mark E. Thompson*,[†]

[†]Department of Chemistry, University of Southern California, Los Angeles, California 90089, United States

[‡]Center for Neutron Research, National Institute of Standards and Technology, Gaithersburg, Maryland 20899, United States

Supporting Information

ABSTRACT: A benzannulated boron dipyrromethene (BODIPY, bDIP) molecule exhibiting strong absorption at 640 nm was synthesized. The organic dye was used in an organic solar cell as the electron donor with C_{60} as the acceptor. The BODIPY dye demonstrated the best performance in lamellar architecture (indium tin oxide (ITO)/bDIP/C_{60}/bathocuproine/Al), giving power conversion efficiency up to 4.5% with short-circuit current (J_{SC}) of 8.7 mA/cm^2 and an open-circuit voltage (V_{OC}) of 0.81 V. Neutron reflectivity experiments were performed on the bilayer film to investigate the thickness dependence of J_{SC}. A 13 nm mixed layer was found to be present at the donor/acceptor interface in the bilayer device, formed when the C_{60} was deposited onto a room temperature bDIP film. Planar-mixed heterojunction devices were fabricated to understand the extent of spontaneous mixing between the donor and acceptor materials. The native mixed region in the bilayer device was shown to most resemble 1:3 bDIP:C_{60} layer in the structure: (ITO/bDIP/bDIP:C_{60} blend/C_{60}/bathocuproine/Al).

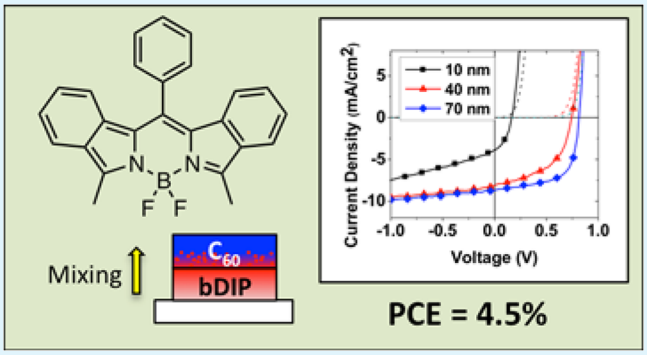

KEYWORDS: *organic photovoltaics, BODIPY, bilayer, planar-mixed heterojunction, neutron reflectivity*

INTRODUCTION

Organic photovoltaics (OPVs) have earned considerable attention in the past decade as a result of their potential to be low-cost, lightweight, and environmentally friendly sources of energy. To achieve high efficiencies, the organic dyes must have high absorptivity, high carrier mobility, and complete coverage of the solar spectrum. Organic small molecules are promising candidates for solar cells because they can be modified easily to provide these ideal properties. Given these advantages, small-molecule based OPVs have been reported with power conversion efficiencies (PCE) > 8%.[1−4] One effective strategy to improve the PCE is by increasing the amount of visible and near-infrared (NIR) photons harvested. Since a substantial portion of the solar flux lies in the visible and NIR regions, a higher short-circuit current (J_{SC}) can be obtained by focusing on these optically dense regions, leading to a device with higher PCE.

Boron dipyrromethenes, or BODIPYs (Scheme 1), are a class of materials well-suited to this strategy for improving OPV performance. The high optical density and efficient luminescence observed for BODIPYs make them ideal for a wide range of applications,[5−7] including biological labeling agents, chemical sensors, and laser dyes. Though many π-conjugated red/NIR BODIPYs have been reported[8−11] in the literature, only a handful have been applied to photovoltaics,[12−16] including a BODIPY-based bulk heterojunction (BHJ) device with a PCE of 4.7%.[17] Here, we investigate bilayer and planar-mixed heterojunction (PMHJ) device architectures incorporating a benzannulated BODIPY (bDIP), shown in Scheme 1, as an electron donor.

Scheme 1

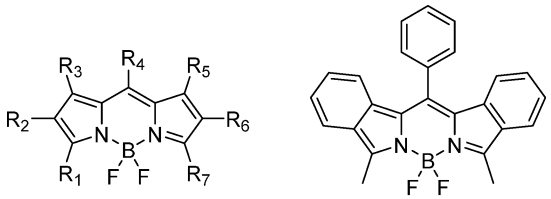

MATERIAL PROPERTIES

The synthesis of bDIP was first reported by Ono and coworkers.[18] The extended π-system leads to a broader absorption in the red region of the solar spectrum than the analogous BODIPY compounds. Solution-phase photophysical measurements of bDIP in dichloromethane show absorption and emission maxima occur at 602 and 610 nm, respectively (Figure 1).[18] Photophysical measurements of the neat thin film

Received: October 7, 2014
Accepted: December 12, 2014
Published: December 12, 2014

DOI: 10.1021/am506874k
ACS Appl. Mater. Interfaces 2015, 7, 662−669

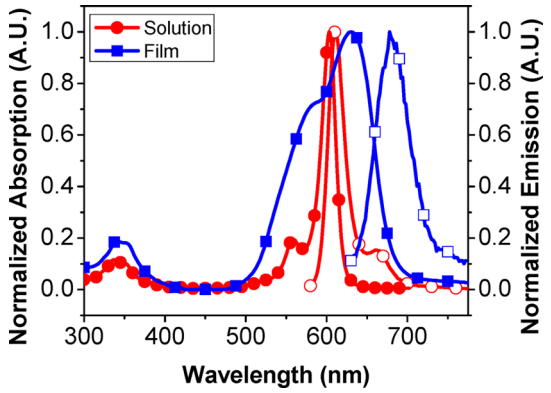

Figure 1. Absorption (solid shapes) and emission (hollow shapes) of bDIP taken in dichloromethane solution and thin film on a quartz substrate.

show a marked bathochromic shift of the absorption maximum to 640 nm with substantial broadening of the peak, and an absorption coefficient of 3.03×10^5 cm^{-1} at λ_{max}. The red shift and broadening relative to solution spectra are likely the result of strong $\pi-\pi$ stacking of adjacent molecules. Strong intermolecular interactions are seen in the crystal packing of bDIP, which shows significant overlap of the benzannulated rings of adjacent bDIPs with a π-to-π spacing of 3.45 Å.[18] The thin film sample gives a large Stokes shift of the emission in the thin film at 680 nm. Consistent with previously reported values, bDIP gives reversible oxidation and reduction waves in the cyclic voltammogram, with potentials of 0.395 and −1.70 V versus ferrocene, respectively.[18] The highest occupied molecular orbital (HOMO) and lowest unoccupied molecular orbital (LUMO) of bDIP were calculated using reported methods[19,20] and are shown in Figure2a, relative to C_{60}.[21] The energy level alignment of bDIP makes a suitable donor to be coupled with C_{60} as the electron acceptor in an OPV.

Bilayer Photovoltaic Devices. Bilayer OPVs were fabricated with the structure: indium tin oxide (ITO)/bDIP (10−110 nm)/C_{60} (40 nm)/bathocuproine (10 nm)/Al (100 nm), shown in Figure 2a. The current density versus voltage plots for these bDIP-based OPVs are presented in Figure 2b, and the relevant parameters are summarized graphically in Figure 3. Excluding the 10 nm device, the open-circuit voltage (V_{OC}) observed for bDIP/C_{60} devices are high, falling between 0.74 and 0.81 V. The J_{SC} improves with increasing thicknesses of the bDIP donor layer, starting from 3.9 mA/cm^2 at bDIP = 10 nm to a maximum current of 8.7 mA/cm^2 for the 70 nm

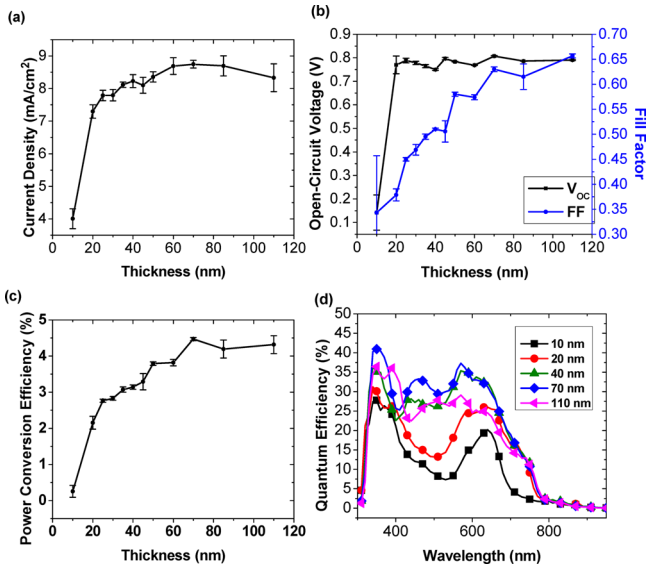

Figure 3. PV performance of bilayer bDIP:C_{60} devices with different thickness, (a) current densities, (b) V_{OC} and FF, (c) PCE, and (d) EQE. The error bars represent device-to-device variations for each parameter at the given thickness. Some error bars are too small to be seen in the plot.

bDIP device. Poor performing devices were observed for OPVs with bDIP donor layer thicknesses of 10−40 nm, due principally to low fill factor (FF). The 10 nm donor layer gives a very low V_{OC} and FF, with a $J-V$ trace very similar to that of a simple C_{60} junction, that is, ITO/C_{60}/Al.[22] It is likely that the 10 nm bDIP film is not continuous and that the low voltage is due to direct C_{60}/ITO contacts.

External quantum efficiency (EQE) plots are shown in Figure 3d. Strong photoresponse from bDIP and C_{60} are seen at 570/780 nm and 340/450 nm, respectively. Similar to the trend seen in J_{SC}, there was minimal enhancement in EQE when increasing the thickness from 40 to 70 nm.

The FFs change proportionally with bDIP thickness up to roughly 50 nm, suggesting that these devices have improved charge conduction or induced favorable morphology with thicker bDIP layers. The conduction is facilitated by the $\pi-\pi$ interaction between the fused benzene rings, which is expected to enhance the carrier-hopping rate. The origin and impact of this improvement will be discussed further below. Despite being limited by the bilayer structure, the best performing bilayer device (70 nm) achieved a PCE of 4.5%.

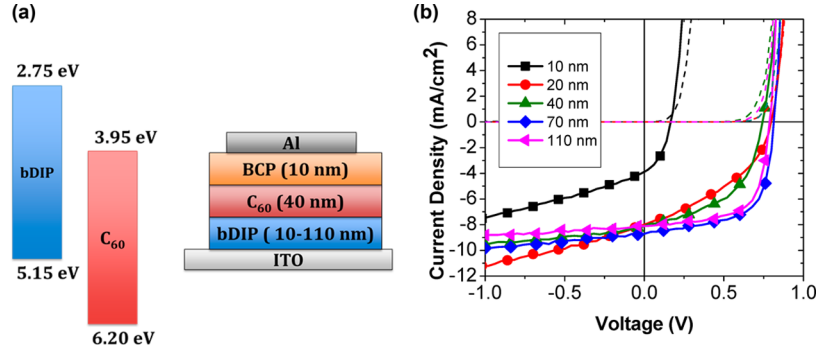

Figure 2. (a) Device architecture of bilayer bDIP:C_{60} device and calculated HOMO/LUMO. (b) Representative $J-V$ curves under light (solid lines) and dark (dashed lines) conditions. Some curves omitted for clarity.

DOI: 10.1021/am506874k
ACS Appl. Mater. Interfaces 2015, 7, 662−669

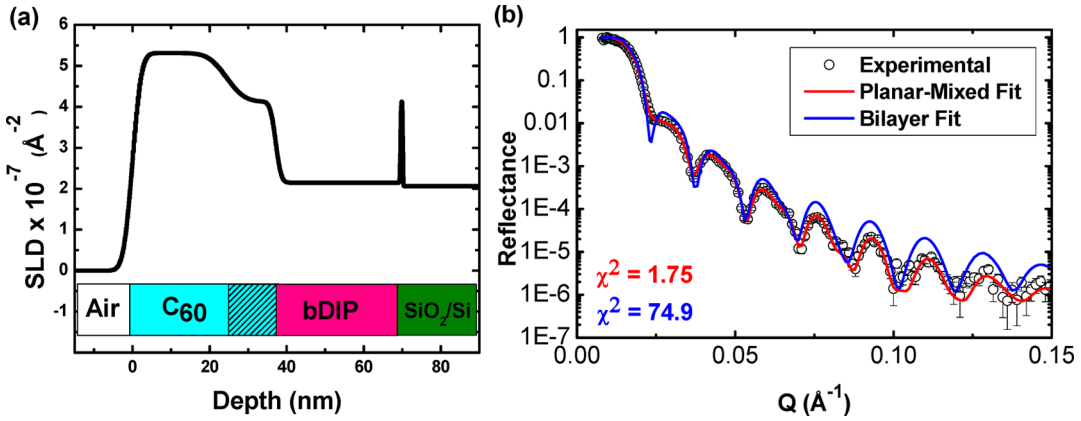

Figure 4. NR reflectance (black circles), with error bars, of the film stack: C_{60} (30 nm)/bDIP (30 nm)/SiO_2/Si is shown here (b). Overlaid on the data is the simulated reflectance spectrum and its χ^2 value of the discrete bilayer (blue trace), and intermixed three layer model (red trace). In part (a) the three layer model film stack's SLD vs depth profile is shown. In this plot the air/C_{60} interface is taken as 0.

While the J_{SC} increases with bDIP thickness, it is important to note that the increase in J_{SC} is not linearly correlated to the bDIP thickness. A doubling of the bDIP, from 35 to 70 nm, increases the photocurrent by less than 10%. Furthermore, at thicknesses greater than 70 nm, J_{SC} decreases with increasing bDIP. The drop in J_{SC} upon increasing the bDIP layer beyond 70 nm is expected, since the bDIP that is farther than the exciton diffusion length from the donor/acceptor (D/A) interface contributes to absorption but does not generate a photocurrent. This results in filtering some of the light from reaching the "active" bDIP near the C_{60} layer. This phenomenon has been seen for other highly absorbing dyes, such as squaraines.[23] Optical fields of the devices (Supporting Information, Figure S1) were modeled using transfer-matrix formalism[24,25] for different thicknesses to investigate the effects of optical interferences. Red photons were shown to be concentrated near the ITO/bDIP interfaces; however, the calculated reduced photocurrents do not agree with experimental observations of increasing J_{SC}. While a gradual decrease in J_{SC} with donor thickness is expected for thick donor layers, the near insensitivity to donor thickness between 35 and 70 nm is not expected. We believe that the insensitivity of J_{SC} to donor thickness is due to the structure of the D/A interface and will discuss this further below.

Neutron Reflectivity. The device representation in Figure 2a, which is typical for describing lamellar OPVs, suggests that the organic layers are uniform and that sharp interfaces exist between donor and acceptor. Recent studies have suggested that this picture may not be correct for D/A materials that interact strongly.[26−29] We have carried out neutron reflectivity (NR) measurements[30] on a bDIP/C_{60} bilayer to determine the structure at the D/A interface directly, in a manner analogous to what has been reported for other organic bilayer systems.[31−34] The sample was prepared via thermal vapor deposition at 2 Å/s on a silicon wafer with the structure: Si/SiO_2/bDIP (30 nm)/C_{60} (30 nm). Model film stacks were generated, and the reflectance spectra were calculated. The model stacks were evaluated by analyzing the calculated spectra with a chi-squared (χ^2) method for goodness of fit to the measured reflectance spectrum.[35] We started with a bilayer model, similar to the cartoon in Figure 2a. The layer thickness and surface roughness were allowed to vary but, as seen in Figure 4b (blue trace), we were unable to converge on a good fit, getting a minimum χ^2 value of 74.9. However, upon the inclusion of a blended layer in a three-layer model to fit the data (Figure 4b), the calculated spectrum converged well on the measured reflectance, giving a χ^2 value of 1.75. The film stack model in Figure 4a is tabulated in Table 1.

Table 1. Modeled SLD, Thicknesses, and Roughness of Each Component Layer for a Stack Including a Mixed C_{60}:bDIP Layer As Shown in Figure 5a

layer	SLD ($Å^{-2}$)	thickness (nm)	roughness (nm)
C_{60}	5.28×10^{-06}	24	4
mixed layer	3.94×10^{-06}	13	10
bDIP	2.11×10^{-06}	33	30
SiO_2	4.10×10^{-06}	0.6	0.3
Si	2.06×10^{-06}	∞	0.6

The fitted model to the NR data suggests that there is a substantial amount of mixing at the interface between bDIP and C_{60}, despite our attempt to deposit discrete layers. The neat C_{60} and bDIP layers have thicknesses of ~24 ± 1 nm and 33 ± 1 nm, respectively, and the mixed layer has a thickness of 13 ± 1 nm and a roughness of 10 nm. The roughness, which is nearly on the same order as the thickness of the mixed layer, generates a region of continuously changing scattering length density (SLD) from an unknown C_{60}:bDIP ratio at the interface to pure C_{60} deeper in the film.

The 10 nm difference between the thickness obtained from crystal monitors of the deposition system and NR measurement can be accounted for by the change in density between the mixed region and the pristine materials. The thickness of each pure material is calibrated via ellipsometry prior to deposition, but these thicknesses do not account for a mixture. The mixed layer is less dense than the pure materials themselves; hence, a higher volume and total thickness are observed. Thus, the total amount of matter deposited remains the same as 30 nm of each material, while the thicknesses fluctuate due to lower density.

To corroborate that the extent of mixing is not a continuation of ITO or Si substrate roughness, the root-mean-square roughness (r_{rms}) of bare substrates were obtained from atomic force microscopy (AFM) as 0.20 and 0.60 nm, respectively. AFM rules out the cause of the intermixing as a consequence of the substrate roughness, which is 2 orders of magnitude smaller. Furthermore, NR experiment done on a thicker stack of Si/SiO_2/bDIP (60 nm)/C_{60} (40 nm), shown in

DOI: 10.1021/am506874k
ACS Appl. Mater. Interfaces 2015, 7, 662−669

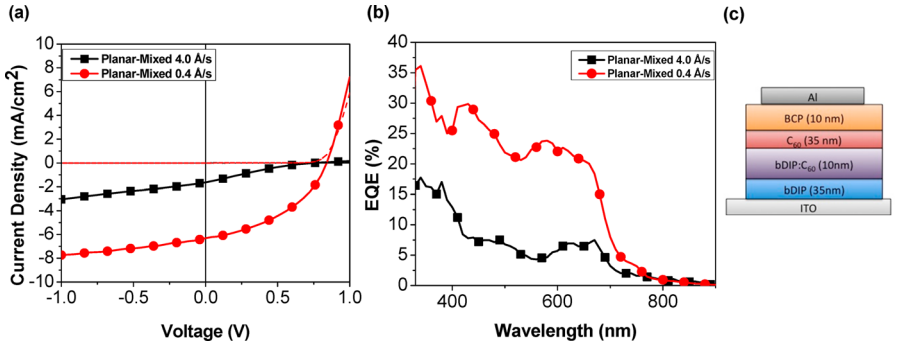

Figure 5. Representative $J-V$ curves (a) under light (solid lines) and dark (dashed lines) conditions, EQE (b), and device structure (c) of rate-dependent planar-mixed heterojunction devices.

Supporting Information, Figure S2, reveals a similar intermixed layer thickness of 14 nm that is independent of bDIP or C_{60} thickness. This model suggests that during the second C_{60} deposition, the hot C_{60} subliming at 490 °C dissolves some bDIP (mp = 310 °C) into the C_{60} layer at some preferred ratio that tails off as the layer gets thicker and diffusion of bDIP stops.

This result is consistent with the lower V_{OC} for 10 nm bDIP devices. Since the mixed region of C_{60} and bDIP is on the order of 13 nm, these devices are likely to be largely if not entirely composed of a single intermixed layer even though the components were separately deposited. Thus, C_{60}/ITO contact is unavoidable, as the formation of a neat bDIP layer cannot be achieved, leading to lower V_{OC} values. Complete bDIP coverage can also explain the improvement in FF with increasing bDIP thickness. Given that the thinner devices have a substantial portion of the film as a mixed layer, it should be less efficient at shuttling carriers to the electrodes than their pristine counter parts. As the neat bDIP layer gets thicker, it accounts for a higher percentage of the device and transports holes more effectively and serves as a better electron-blocking layer than the blended layer.

The presence of a 13 nm mixed layer also explains the lack of a substantial increase (or decrease) in J_{SC} as the bDIP is made thicker. Since the thickness of the mixed interfacial layer does not change with the thickness of bDIP layer underneath it, the underlying factors responsible for photocarrier generation may also remain unchanged. If bDIP has a limited exciton diffusion length (L_D) and J_{SC} is dominated by photons absorbed near and inside of the blended region, the observed small differences in J_{SC} can be attributed to a constant baseline photocurrent from the near and intermixed region with minor contributions from bDIP beyond the mixed region.

Planar-Mixed Heterojunction Photovoltaic Devices. To understand the nature of the intermixed layer, OPVs were prepared with a mixed bDIP–C_{60} layer between neat bDIP and C_{60} layers, forming a planar-mixed heterojunction (PMHJ) device. In several studies, PMHJ devices have been shown to be the optimal architecture, outperforming their bulk heterojunction (BHJ) or planar heterojunction counterparts.[36−39] The addition of the mixed phase can lead to an enhancement in J_{SC} via an increase in the interfacial area between the donor and acceptor.[40−42] The first planar-mixed heterojunction device consists of a thin layer of 1:1 bDIP/C_{60} blend, that is, ITO/bDIP 35 nm/mixed-bDIP–C_{60} 10 nm/C_{60} 35 nm/BCP/Al, as shown in Figure 5c. The total amount of bDIP deposited was the same as that in a 40 nm bDIP bilayer OPV, used as control for comparison. The mixed layer was deposited at rates of either 4.0 or 0.4 Å/s, while the other organic layers were deposited at 2 Å/s, the same rate used for the bilayer control. The PMHJ devices prepared at a high deposition rate perform poorly compared to the bilayer control (Table 2). The

Table 2. Summary of PV Parameters for Rate-Dependent PMHJ Devices and the Control Bilayer of Structure: ITO/bDIP/C_{60}/BCP/Al

rate (Å/s)	J_{SC} (mA/cm^2)	V_{OC} (V)	FF	η (%)
P-M 4.0 Å/s	1.49	0.75	0.20	0.23
P-M 0.4 Å/s	6.32	0.84	0.42	2.25
bilayer	8.11	0.79	0.51	3.06

performance of the PMHJ device improved significantly when the mixed layer was deposited at the slower rate, increasing J_{SC}, V_{OC}, and FF, leading to a PCE of 2.3% for the 0.4 Å/s device. The EQE, as shown in Figure 5b, reflects these enhancements with at least 2-fold increase in photoresponse across all wavelengths.

Though the total amount of material in the mixed layers is identical, the spectral response of the devices prepared at high and low deposition rates are not the same. The relative C_{60} and bDIP responses for the two devices differ. In Figure 5b, the device prepared with a high deposition rate shows weaker C_{60} response (400–550 nm) relative to its bDIP response (550–725 nm) than is seen for the device prepared at a slow deposition rate. It has been shown that the C_{60} absorption between 400 and 550 nm is due to an intermolecular charge-transfer (CT) and depends strongly on the C_{60} concentration in mixed thin films.[43,44] The C_{60} CT absorbance of a mixed film decreases exponentially with the amount of dopant. A film composed of a homogeneous 1:1 mixture shows a decrease in CT absorption of 40% relative to a neat thin film of C_{60}. The marked decrease in CT absorbance observed when the mixed layer is deposited at 4.0 Å/s suggests that the bDIP–C_{60} film is intimately mixed. In contrast, the film prepared at the slower deposition rate shows a clear peak at 450 nm, consistent with separate and crystalline domains of bDIP and C_{60} in the thin film.

AFM was used to investigate the effect of deposition rate on the morphology of these blended films, as shown in Figure 6. Films of the 4.0 and 0.4 Å/s intermixed layer deposited on a substrate consisting of 35 nm of bDIP on ITO were scanned. Compared to neat bDIP and C_{60} with r_{rms} = 1.53 nm and r_{rms} = 0.84 nm, respectively, the film prepared with a 4.0 Å/s rate gives a lower root-mean-square roughness, r_{rms} = 1.43 nm, than the one prepared at 0.4 Å/s, with r_{rms} = 2.35 nm. The average

DOI: 10.1021/am506874k
ACS Appl. Mater. Interfaces 2015, 7, 662–669

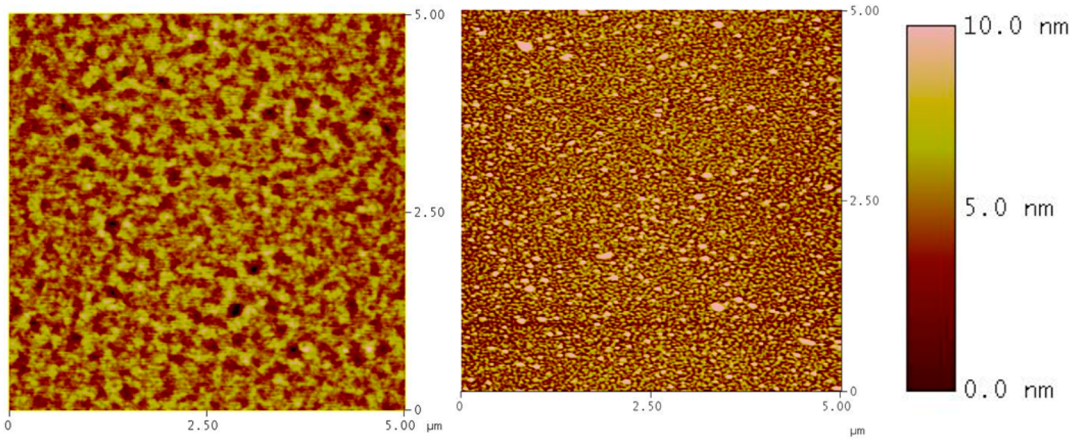

Figure 6. AFM images of 1:1 bDIP:C_{60} films with different deposition rates: 4.0 Å/s (left), r_{rms} = 1.43 nm and 0.4 Å/s (right), r_{rms} = 2.35 nm. The images are 5.00 μm by 5.00 μm.

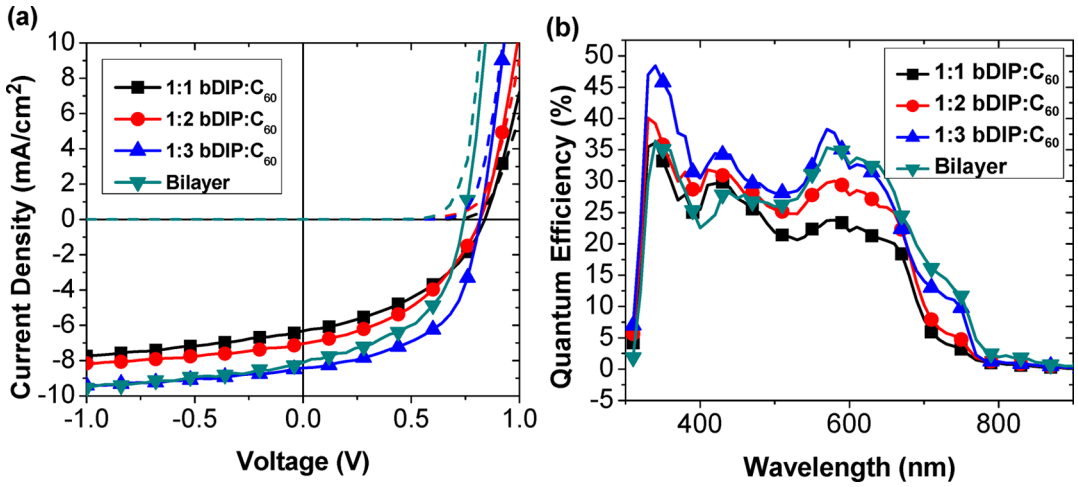

Figure 7. Representative *J*–*V* curves (a) under light (solid lines) and dark (dashed lines) conditions, and EQE (b) of ratio-dependent planar-mixed heterojunction devices.

domain sizes of these two films are drastically different. At 4.0 Å/s, a larger length for the phase-separated feature at ~0.4 μm is observed compared to ~0.1 μm for the 0.4 Å/s film. A rougher film with smaller domains suggests that more interfacial area is available for exciton dissociation, which can improve device performance. Despite these considerable improvements, the resulting 2.3% PCE is still below that of the bilayer control device.

Varying the ratio of bDIP and C_{60} in the mixed layer gave PMHJ devices with a similar PCE to the bilayer device. Three PMHJ devices were examined, shown in Figure 7, with different intermixed layer bDIP:C_{60} ratios (1:1,1:2, and 1:3) that were deposited at a constant rate of 0.2 Å/s for bDIP and 0.2 Å/s to 0.6 Å/s for the different C_{60} ratios. All bDIP PMHJ devices have $V_{OC} \approx 0.82$ V, which is higher than that of the bilayer control. As the mixed layer becomes more C_{60}-rich, J_{SC} and FF both increase, leading to an overall improvement in PCE from 2.3% for the 1:1 device to 3.8% for the 1:3 device. As listed in Table 3, the 1:3 ratio device most closely represents the bilayer device. The PMHJ 1:3 device generally outperforms the bilayer analogue. Their respective values for J_{SC} are 8.42 mA/cm^2 versus 8.11 mA/cm2; a V_{OC} of 0.82 V comparable to 0.79 V; and an FF value of 0.55 instead of 0.51.

Table 3. Summary of PV Parameters for Ratio-Dependent PMHJ Devices and the Control Bilayer of Structure: ITO/bDIP/C_{60}/BCP/Al

ratio (bDIP:C_{60})	J_{SC} (mA/cm^2)	V_{OC} (V)	FF	η (%)
1:1	6.32	0.84	0.42	2.25
1:2	7.04	0.82	0.43	2.49
1:3	8.42	0.82	0.55	3.76
bilayer	8.11	0.79	0.51	3.06

The EQE plot in Figure 7b shows the photoresponse of bDIP from 550 to 780 nm increasing with C_{60} concentration, nearly overlapping with the bilayer trace in this region at 1:3 ratio. The presence of a red shoulder at ~750 nm, which is absent at lower C_{60} loading, also reinforces the interfacial similarity between the 1:3 PMHJ and bilayer device. The main contribution to the superior 1:3 PMHJ over the bilayer is clearly shown from the higher C_{60} photoresponse ranging from 350 to 525 nm. The 1:3 PMHJ has ~13% higher EQE than the bilayer, which is likely the origin of the increase in J_{SC}. These effects result in a 25% improvement in PCE from the bilayer device when preparing an intentionally mixed PMHJ of a given thickness and further confirm that even in a bilayer device, the interface is not discrete.

DOI: 10.1021/am506874k
ACS Appl. Mater. Interfaces 2015, 7, 662–669

CONCLUSION

We have demonstrated the use of a π-extended BODIPY dye in OPV devices to successfully harvest red/NIR photons out to 800 nm. The best device showed a PCE of 4.5% in a bilayer structure. The observed insensitivity of the bilayer devices to bDIP thickness is due to the existence of an inherent mixed layer at the D/A interface. Though each material was deposited separately during fabrication of the lamellar devices, spontaneous mixing of C_{60} and bDIP was unavoidable. NR experiment estimates the thickness of the mixed layer between C_{60} and bDIP to be approximately 13 nm. This layer acts as the primary photocurrent generator and significantly impacts the PCE. We show that deposition rate, morphology, and composition of the mixed layer are important factors governing device PCE. We were able to replicate the "bilayer" device by intentionally introducing a mixed layer in PMHJ devices. PMHJ devices with a slower deposition rate in the intermixed layer results in a higher PCE due to different morphology. The PV performances of devices with different blend ratios reveal that the natively mixed region has a bDIP:C_{60} ratio close to that of 1:3. Contrary to what is usually expected when fabricating a bilayer device, an unintentional blended layer may be present in lamellar devices. The thickness will vary depending on the miscibility of the two components. The PMHJ-like picture was clearly the best representation of bDIP/C_{60}-based OPVs and may be the most realistic representation of the majority of lamellar devices.

EXPERIMENTAL SECTION

Unless noted otherwise, all chemicals were purchased from Sigma-Aldrich and used without further purification. Dry solvents were purified using a Glass Contour Solvent System, and all reactions were performed under inert nitrogen atmosphere. bDIP was prepared as reported by Ono and co-workers starting from a retro-Diels–Alder isoindole precursor followed by a standard BODIPY synthesis.[18,45] The resulting bronze-colored solids were purified by recrystallization.

Thin-film absorption was taken from a vacuum-deposited film of bDIP on quartz. UV–vis spectra were recorded on a Hewlett-Packard 4853 Diode Array Spectrometer. Cyclic voltammetry (CV) measurements were performed using an EG&G Potentiostat/Galvanostat model 283. Samples were run in 0.1 M tetra-*n*-butyl-ammonium hexafluorophosphate solution in dichloromethane purged with nitrogen. The counter, reference, and working electrodes were platinum, silver, and glassy carbon, respectively. Scans were performed at 100 mV/s, and oxidation/reduction values were calibrated to ferrocene/ferrocenium internal references.

AFM measurements were taken on a Dimension Icon Scanning Probe Microscope (Bruker) with PeakForce tapping mode. A Scan Asyst-Air Tip (Bruker) was used to scan the 5 μm × 5 μm images. Image processing and domain-size analysis were performed with Nanoscope Analysis software.

Organic and aluminum layers were deposited via vacuum thermal deposition chamber (Angstrom Engineering) at 2 Å/s per source under pressure of 10^{-6} Torr. bDIP, C_{60} (MTR Limited), and bathocuproine (BCP) (Aldrich) were purified by thermal gradient sublimation. Device structure of the cells are as follows: ITO/X/BCP (10 nm)/Al (100 nm); where X = bDIP (10–110 nm)/C_{60} (40 nm) for thickness dependence films or X = bDIP (35 nm)/1:1–1:3 ratio bDIP:C_{60} (10 nm)/C_{60} (35 nm) for PMHJ. Fast and slow rate PMHJ devices were made with a net rate of 4.0 Å/s with 2.0 Å/s from each bDIP and C_{60} source, or 0.4 Å/s with 0.2 Å/s source rates, respectively. Concentration-dependent devices were fabricated with a constant rate of bDIP at 0.2 Å/s and varying the rate of C_{60} from 0.2 Å/s to 0.4 Å/s or 0.6 Å/s for 1:1, 1:2, and 1:3 bDIP:C_{60}, respectively. ITO (Thin Films, Inc.) substrates were rinsed with Tergitol and boiled in each of the organic solvents, namely, tetrachloroethylene, acetone, and alcohol, for 5 min each. A 10 min UV–ozone treatment prior loading into the vacuum chamber followed. After the deposition of organic materials on ITO, a mask with 1 mm diameter openings was placed on the substrate followed by a deposition of aluminum (100 nm) from aluminum shots (Alfa).

Current–voltage characteristics were tested in dark and illumination under simulated AM 1.5 G filter adjusted to 1 sun intensity (100 mW/cm^2) with a silicon photodiode calibrated by the National Renewable Energy Laboratory. Spectral response was measured using a monochromatic light source. Spectral mismatch and device efficiencies were calculated following standard procedure.[46] The PV parameters of all devices reported were averaged over at least three devices and over at least eight devices for those ranging from 20 to 60 nm. Statistical analysis was performed to obtain the average values and standard errors for the reported data.

Sample film stacks for NR measurements were made by thermal vapor evaporation onto silicon wafers with a native oxide layer on their surface. These stacks were prepared in a nitrogen atmosphere and measured in air at the National Institute of Standards and Technology using their NG-7 Horizontal Neutron Reflectometer. The programs from the reflpak suite were used for elements of the data reduction and fitting film stack models to the reflectometry spectra.[35]

ASSOCIATED CONTENT

Supporting Information

Optical field modeling of bilayer devices and additional NR measurements. This material is available free of charge via the Internet at http://pubs.acs.org.

AUTHOR INFORMATION

Corresponding Author

*E-mail: met@usc.edu.

Notes

The authors declare the following competing financial interest(s): M.T. has a financial interest in one of the sponsors of this work, namely, Nanoflex Power Corporation.

ACKNOWLEDGMENTS

We would like to acknowledge the Nanoflex Power Corporation and the Center for Advanced Molecular Photovoltaics (CAMP) (KUS-C1-015-21) of the King Abdullah University of Science and Technology (KAUST) for financial support of this work.

REFERENCES

(1) Lin, Y.; Li, Y.; Zhan, X. Small Molecule Semiconductors for High-Efficiency Organic Photovoltaics. *Chem. Soc. Rev.* **2012**, *41* (11), 4245–4272.

(2) Zhou, J.; Zuo, Y.; Wan, X.; Long, G.; Zhang, Q.; Ni, W.; Liu, Y.; Li, Z.; He, G.; Li, C.; Kan, B.; Li, M.; Chen, Y. Solution-Processed and High-Performance Organic Solar Cells Using Small Molecules with a Benzodithiophene Unit. *J. Am. Chem. Soc.* **2013**, *135* (23), 8484–8487.

(3) Kyaw, A. K. K.; Wang, D. H.; Gupta, V.; Leong, W. L.; Ke, L.; Bazan, G. C.; Heeger, A. J. Intensity Dependence of Current–Voltage Characteristics and Recombination in High-Efficiency Solution-Processed Small-Molecule Solar Cells. *ACS Nano* **2013**, *7* (5), 4569–4577.

(4) Cnops, K.; Rand, B. P.; Cheyns, D.; Verreet, B.; Empl, M. A.; Heremans, P. 8.4% Efficient Fullerene-Free Organic Solar Cells Exploiting Long-Range Exciton Energy Transfer. *Nat. Commun.* **2014**, *5*, 1–6.

(5) Benstead, M.; Mehl, G. H.; Boyle, R. W. 4,4′-Difluoro-4-Bora-3a,4a-Diaza-S-Indacenes (Bodipys) as Components of Novel Light Active Materials. *Tetrahedron* **2011**, *67* (20), 3573–3601.

(6) Ulrich, G.; Ziessel, R.; Harriman, A. The Chemistry of Fluorescent Bodipy Dyes: Versatility Unsurpassed. *Angew. Chem., Int. Ed.* **2008**, *47* (7), 1184–1201.

DOI: 10.1021/am506874k
ACS Appl. Mater. Interfaces 2015, 7, 662–669

(7) Loudet, A.; Burgess, K. Bodipy Dyes and Their Derivatives: Syntheses and Spectroscopic Properties. *Chem. Rev.* **2007**, *107* (11), 4891−4932.
(8) Sarma, T.; Panda, P. K.; Setsune, J.-i. Bis-Naphthobipyrrolylmethene Derived Bodipy Complex: An Intense near-Infrared Fluorescent Dye. *Chem. Commun.* **2013**, *49*, 9806−9808.
(9) Ulrich, G.; Goeb, S. b.; De Nicola, A.; Retailleau, P.; Ziessel, R. Chemistry at Boron: Synthesis and Properties of Red to near-Ir Fluorescent Dyes Based on Boron-Substituted Diisoindolomethene Frameworks. *J. Org. Chem.* **2011**, *76* (11), 4489−4505.
(10) Kowada, T.; Yamaguchi, S.; Fujinaga, H.; Ohe, K. Near-Infrared Bodipy Dyes Modulated with Spirofluorene Moieties. *Tetrahedron* **2011**, *67* (17), 3105−3110.
(11) Jiao, C.; Huang, K.-W.; Wu, J. Perylene-Fused Bodipy Dye with near-Ir Absorption/Emission and High Photostability. *Org. Lett.* **2011**, *13* (4), 632−635.
(12) Kim, B.; Ma, B.; Donuru, V. R.; Liu, H.; Frechet, J. M. J. Bodipy-Backboned Polymers as Electron Donor in Bulk Heterojunction Solar Cells. *Chem. Commun.* **2010**, *46* (23), 4148−4150.
(13) Kubo, Y.; Watanabe, K.; Nishiyabu, R.; Hata, R.; Murakami, A.; Shoda, T.; Ota, H. Near-Infrared Absorbing Boron-Dibenzopyrromethenes That Serve as Light-Harvesting Sensitizers for Polymeric Solar Cells. *Org. Lett.* **2011**, *13* (17), 4574−4577.
(14) Kolemen, S.; Bozdemir, O. A.; Cakmak, Y.; Barin, G.; Erten-Ela, S.; Marszalek, M.; Yum, J.-H.; Zakeeruddin, S. M.; Nazeeruddin, M. K.; Gratzel, M.; Akkaya, E. U. Optimization of Distyryl-Bodipy Chromophores for Efficient Panchromatic Sensitization in Dye Sensitized Solar Cells. *Chem. Sci.* **2011**, *2* (5), 949−954.
(15) Rousseau, T.; Cravino, A.; Ripaud, E.; Leriche, P.; Rihn, S.; De Nicola, A.; Ziessel, R.; Roncali, J. A Tailored Hybrid Bodipy-Oligothiophene Donor for Molecular Bulk Heterojunction Solar Cells with Improved Performances. *Chem. Commun.* **2010**, *46* (28), 5082−5084.
(16) Poe, A. M.; Della Pelle, A. M.; Subrahmanyam, A. V.; White, W.; Wantz, G.; Thayumanavan, S. Small Molecule Bodipy Dyes as Non-Fullerene Acceptors in Bulk Heterojunction Organic Photovoltaics. *Chem. Commun. (Cambridge, U.K.)* **2014**, *50* (22), 2913−2915.
(17) Bura, T.; Leclerc, N.; Fall, S.; Lévêque, P.; Heiser, T.; Retailleau, P.; Rihn, S.; Mirloup, A.; Ziessel, R. High-Performance Solution-Processed Solar Cells and Ambipolar Behavior in Organic Field-Effect Transistors with Thienyl-Bodipy Scaffoldings. *J. Am. Chem. Soc.* **2012**, *134* (42), 17404−17407.
(18) Shen, Z.; Röhr, H.; Rurack, K.; Uno, H.; Spieles, M.; Schulz, B.; Reck, G.; Ono, N. Boron−Diindomethene (Bdi) Dyes and Their Tetrahydrobicyclo Precursors—En Route to a New Class of Highly Emissive Fluorophores for the Red Spectral Range. *Chem.—Eur. J.* **2004**, *10* (19), 4853−4871.
(19) D'Andrade, B. W.; Datta, S.; Forrest, S. R.; Djurovich, P.; Polikarpov, E.; Thompson, M. E. Relationship between the Ionization and Oxidation Potentials of Molecular Organic Semiconductors. *Org. Electron.* **2005**, *6* (1), 11−20.
(20) Djurovich, P. I.; Mayo, E. I.; Forrest, S. R.; Thompson, M. E. Measurement of the Lowest Unoccupied Molecular Orbital Energies of Molecular Organic Semiconductors. *Org. Electron.* **2009**, *10* (3), 515−520.
(21) Wilke, A.; Endres, J.; Hormann, U.; Niederhausen, J.; Schlesinger, R.; Frisch, J.; Amsalem, P.; Wagner, J.; Gruber, M.; Opitz, A.; Vollmer, A.; Brutting, W.; Kahn, A.; Koch, N. Correlation between Interface Energetics and Open Circuit Voltage in Organic Photovoltaic Cells. *Appl. Phys. Lett.* **2012**, *101* (23), 233301−4.
(22) Taima, T.; Chikamatsu, M.; Bera, R. N.; Yoshida, Y.; Saito, K.; Yase, K. Insertion of Thin Interlayers under the Negative Electrode of C_{60} Schottky-Type Photovoltaic Cells. *J. Phys. Chem. B* **2003**, *108* (1), 1−3.
(23) Wang, S.; Mayo, E. I.; Perez, M. D.; Griffe, L.; Wei, G.; Djurovich, P. I.; Forrest, S. R.; Thompson, M. E. High Efficiency Organic Photovoltaic Cells Based on a Vapor Deposited Squaraine Donor. *Appl. Phys. Lett.* **2009**, *94* (23), 233304−3.
(24) Pettersson, L. A. A.; Roman, L. S.; Inganas, O. Modeling Photocurrent Action Spectra of Photovoltaic Devices Based on Organic Thin Films. *J. Appl. Phys.* **1999**, *86* (1), 487−496.
(25) Peumans, P.; Yakimov, A.; Forrest, S. R. Small Molecular Weight Organic Thin-Film Photodetectors and Solar Cells. *J. Appl. Phys.* **2003**, *93* (7), 3693−3723.
(26) Collins, B. A.; Gann, E.; Guignard, L.; He, X.; McNeill, C. R.; Ade, H. Molecular Miscibility of Polymer−Fullerene Blends. *J. Phys. Chem. Lett.* **2010**, *1* (21), 3160−3166.
(27) Ma, W.; Tumbleston, J. R.; Wang, M.; Gann, E.; Huang, F.; Ade, H. Domain Purity, Miscibility, and Molecular Orientation at Donor/Acceptor Interfaces in High Performance Organic Solar Cells: Paths to Further Improvement. *Adv. Energy Mater.* **2013**, *3* (7), 864−872.
(28) Treat, N. D.; Brady, M. A.; Smith, G.; Toney, M. F.; Kramer, E. J.; Hawker, C. J.; Chabinyc, M. L. Interdiffusion of Pcbm and P3ht Reveals Miscibility in a Photovoltaically Active Blend. *Adv. Energy Mater.* **2011**, *1* (1), 82−89.
(29) Treat, N. D.; Varotto, A.; Takacs, C. J.; Batara, N.; Al-Hashimi, M.; Heeney, M. J.; Heeger, A. J.; Wudl, F.; Hawker, C. J.; Chabinyc, M. L. Polymer-Fullerene Miscibility: A Metric for Screening New Materials for High-Performance Organic Solar Cells. *J. Am. Chem. Soc.* **2012**, *134* (38), 15869−15879.
(30) Majkrzak, C. F. Neutron Reflectometry Studies of Thin Films and Multilayered Materials. *Acta Phys. Pol., A* **1999**, *96*, 81−99.
(31) Giovanna, F.-C. Neutron Reflectivity at the Solid/Liquid Interface: Examples of Applications in Biophysics. *J. Phys.: Cond. Matter* **2001**, *13* (21), 4973.
(32) Ott, F., Neutron Reflectivity. In *Surface Science Techniques;* Bracco, G.; Holst, B., Eds.; Springer: Berlin Heidelberg, 2013; Vol. *51*, pp 307−332.
(33) Russell, T. P. X-Ray and Neutron Reflectivity for the Investigation of Polymers. *Mater. Sci. Rep.* **1990**, *5* (4), 171−271.
(34) Zhou, X.-L.; Chen, S.-H. Theoretical Foundation of X-ray and Neutron Reflectometry. *Phys. Rep.* **1995**, *257* (4−5), 223−348.
(35) Kienzle, P. A.; O'Donovan, K. V.; Ankner, J. F.; Berk, N. F.; Majkrzak, C. F. Nist Center for Neutron Research Reflectometry Software. http://www.ncnr.nist.gov/reflpak/.
(36) Xue, J.; Rand, B. P.; Uchida, S.; Forrest, S. R. A Hybrid Planar−Mixed Molecular Heterojunction Photovoltaic Cell. *Adv. Mater.* **2005**, *17* (1), 66−71.
(37) Ojala, A.; Burckstummer, H.; Hwang, J.; Graf, K.; von Vacano, B.; Meerholz, K.; Erk, P.; Wurthner, F. Planar, Bulk and Hybrid Merocyanine/C60 Heterojunction Devices: A Case Study on Thin Film Morphology and Photovoltaic Performance. *J. Mater. Chem.* **2012**, *22* (10), 4473−4482.
(38) Peumans, P.; Uchida, S.; Forrest, S. R. Efficient Bulk Heterojunction Photovoltaic Cells Using Small-Molecular-Weight Organic Thin Films. *Nature* **2003**, *425* (6954), 158−162.
(39) Hiramoto, M.; Suemori, K.; Yokoyama, M. Photovoltaic Properties of Ultramicrostructure-Controlled Organic Co-Deposited Films. *Jpn. J. Appl. Phys.* **2002**, *41* (4S), 2763.
(40) Walker, B.; Tamayo, A. B.; Dang, X.-D.; Zalar, P.; Seo, J. H.; Garcia, A.; Tantiwiwat, M.; Nguyen, T.-Q. Nanoscale Phase Separation and High Photovoltaic Efficiency in Solution-Processed, Small-Molecule Bulk Heterojunction Solar Cells. *Adv. Funct. Mater.* **2009**, *19* (19), 3063−3069.
(41) Schünemann, C.; Wynands, D.; Wilde, L.; Hein, M. P.; Pfützner, S.; Elschner, C.; Eichhorn, K.-J.; Leo, K.; Riede, M. Phase Separation Analysis of Bulk Heterojunctions in Small-Molecule Organic Solar Cells Using Zinc-Phthalocyanine and C60. *Phys. Rev. B* **2012**, *85* (24), 245314.
(42) Khlyabich, P. P.; Burkhart, B.; Rudenko, A. E.; Thompson, B. C. Optimization and Simplification of Polymer−Fullerene Solar Cells through Polymer and Active Layer Design. *Polymer* **2013**, *54* (20), 5267−5298.
(43) Bartynski, A. N.; Trinh, C.; Panda, A.; Bergemann, K.; Lassiter, B. E.; Zimmerman, J. D.; Forrest, S. R.; Thompson, M. E.; Fullerene-Based, A. Organic Exciton Blocking Layer with High Electron Conductivity. *Nano Lett.* **2013**, *13* (7), 3315−3320.

DOI: 10.1021/am506874k
ACS Appl. Mater. Interfaces 2015, 7, 662−669

(44) Kazaoui, S.; Minami, N.; Tanabe, Y.; Byrne, H. J.; Eilmes, A.; Petelenz, P. Comprehensive Analysis of Intermolecular Charge-Transfer Excited States in C_{60} and C_{70} Films. *Phys. Rev. B* **1998**, *58* (12), 7689−7700.
(45) Okujima, T.; Jin, G.; Hashimoto, Y.; Yamada, H.; Uno, H.; Ono, N. Synthesis of 4,7-Dihydro-2*H*-Isoindole Derivatives Via Diels−Alder Reaction of Tosylacetylene. *Heterocycles* **2006**, *70* (1), 619−626.
(46) Shrotriya, V.; Li, G.; Yao, Y.; Moriarty, T.; Emery, K.; Yang, Y. Accurate Measurement and Characterization of Organic Solar Cells. *Adv. Funct. Mater.* **2006**, *16* (15), 2016−2023.

DOI: 10.1021/am506874k
ACS Appl. Mater. Interfaces 2015, 7, 662−669